

Numerical modelling of the fluid structure interaction using ALE and SPH: The Hydrodynamic Ram phenomenon.

D. Varas¹, J.A. Artero-Guerrero¹, J. Pernas-Sánchez¹ and J. López-Puente¹

¹ Department of Continuum Mechanics and Structural Analysis, University Carlos III of Madrid. Avda. de la Universidad 30, 28911 Leganés, Madrid, Spain

1 Abstract

This work shows the numerical modelling developed to reproduce the effects of the HRAM phenomenon in different fluid-filled square tubes (aluminum and CFRP) when impacted by steel spherical projectiles at different velocities (600 and 900 m/s) and filling levels (60, 75 and 100%). The simulations are performed using two different techniques for the fluid phase: the ALE and SPH formulations. Experimental tests providing the pressure in different points of the fluid, deformation of the walls and cavity evolution are compared with the numerical results in order to validate the models developed. Once the model is validated, it can be used to reach a better understanding of the phenomenon and to study some possibilities to attenuate the effects of the HRAM on the affected structures.

*KEYWORDS: *Hydrodynamic Ram, ALE, SPH, Numerical modeling, Attenuation.*

2 Introduction

Vulnerability against high-velocity impact loads is a critical issue for the design of aerospace structures due to the fact that aircrafts can be subjected to different types of loads during their service life which may cause a catastrophic failure. The military industry has always been concerned about impacts of warhead fragments or medium calibre projectiles, but other kind of impacts may also be dangerous. Bird strikes or hailstones should be considered due to the high probability of occurrence [1,2]. Also, the ice released from the edge of a propeller blade or runway debris may impact different parts of the fuselage [3,4]. Wings represent the largest exposed area to impact threats of all the vulnerable components of an aircraft, therefore impacts onto a fuel tank inside the wings are considered of special relevance in aircraft vulnerability.

Hydrodynamic Ram (HRAM) is a phenomenon that occurs when a high-energy object penetrates a fluid-filled container. The projectile transfers its momentum and kinetic energy through the fluid to the surrounding structure increasing the risk of excessive structural damage leading to a catastrophic failure. HRAM consists of four principal stages: shock, drag, cavitation and exit, Fig.1. Each stage contributes to structural damage through a different mechanism and to a different extent. When the projectile penetrates the wall, the impact energy is transferred to the fluid generating a high-pressure hemispherical shock wave. During the drag phase, the kinetic energy of the projectile is partially transformed into fluid motion, forming a cavity behind the projectile. This cavity grows and pushes the fluid against tube walls causing its deformation. The expansion and collapse of this cavity is known as the cavitation stage. The exit stage is characterized by the pre-stressed in the exit wall due to the initial shock stage and the subsequent loading of the fluid, which explains why damage and strains are larger in the exit wall than in the entry one.

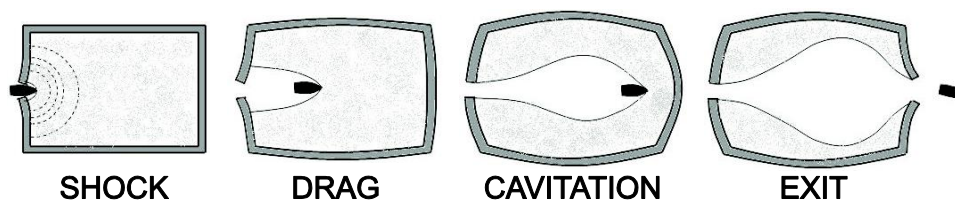


Fig.1: Phases of Hydrodynamic Ram.

The study of the HRAM phenomenon is not only important for the aircraft industry. High velocity impacts on fluid filled containers are of great interest for different industrial fields such as safety of industrial facilities or road haulage. In those cases, an impact in the vessel may produce the failure of the tank with serious consequences on the environment or even toxic and flammability effects.

This work shows the numerical modelling developed to reproduce the effects of the HRAM phenomenon in different fluid filled square tubes (aluminum and CFRP) when impacted by steel spherical projectiles at different velocities and filling levels. The simulations are performed with the finite element code LS-Dyna using two different techniques for the fluid phase: the ALE and SPH formulations. Experimental tests providing the pressure in different points of the fluid, deformation of the walls and cavity evolution are compared with the numerical results in order to assess the validity and accuracy of both ALE and SPH techniques in reproducing such a complex phenomenon. In addition, the numerical model validated has contributed to a better understanding of the phenomenon as well as to study some possibilities to attenuate the effects of the HRAM on the affected structures. With the aim of reducing both the pressure wave generated by the impact and the cavity growing, thin sandwich structures with two metallic skins and a core of air have been located in different positions inside the fluid filled tube. The results show improvements regarding the vulnerability of the fluid filled impacted tubes.

3 Problem description and Finite element model

The geometry and characteristics of the numerical model are based on the experimental tests performed by Varas et al. [5, 6]. The test boxes consisted of 6063-T5 square aluminium tubes (150 mm wide, 2.5 mm thick, and 750 mm long) and square woven CFRP tubes (150 mm wide, 2.2 mm thick and 750 mm long). The composite woven laminate selected was the AGP-193-PW manufactured by Hexcel Composite, composed by 10 plies ($[0]_{10}$). Each ply was made with a plain weave of AS4 carbon fibers and the 8552 epoxy resin. Both boxes were closed with two PMMA windows 30 mm thick, fixed to the specimen with four steel bars; these transparent panels allowed for the recording of the impact process. The projectile was a steel sphere with a diameter of 12.5 mm and a mass of 8 g, launched against the box at two different velocities, 600 and 900 m/s. The boxes were filled at different percentages (60, 75 and 100%) to analyse its influence on the structure response. Pressure data in the fluid was obtained at two different points, PTn (near the impact) and PTf (far from the impact), by means of a PCB 138A06 transducer, their position is shown in Fig. 2.

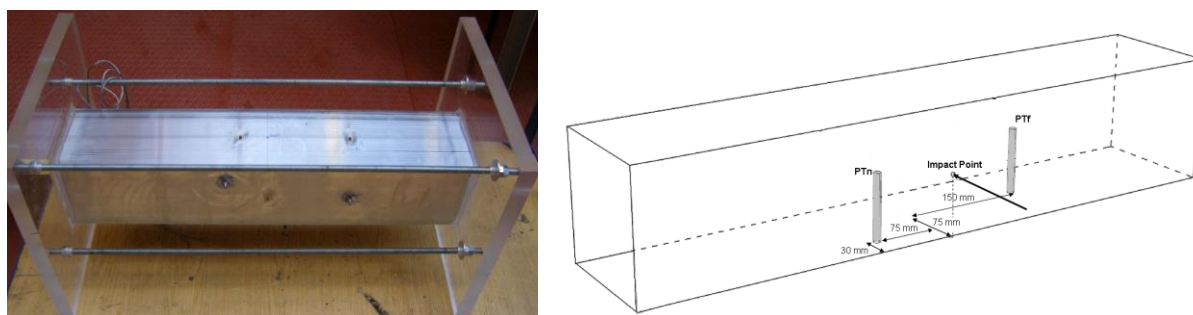


Fig.2: Aluminum tube impacted. Left: experimental set up. Right: sketch of the tube and the position of the pressure transducers.

3.1 Tubes finite element model

Two different material tubes (aluminium and CFRP) have been impacted to study the HRAM effects. The numerical models were developed with the commercial finite element code LS-DYNA v.971 [7].

3.1.1 Aluminium tube

The impacted walls were discretised by means of eight-node solid hexahedron Lagrangian elements with reduced integration. A refined mesh, corresponding to the impact zone, and a progressively coarser mesh as the distance to the hit point grows has been chosen to reproduce accurately the

effects of the HRAM on the tube walls. The impacted walls present five elements through the thickness and an element of 1 mm in size in the other two directions near the impacted zone. Based on previous simulations, the mesh size was considered appropriate to reproduce the behaviour of the solids in the impacted zone. Four-node Belytschko–Tsay shell elements were used to discretise the lateral wall in order to reduce the number of elements. The Johnson–Cook hardening relation (***MAT_015**) was selected to model the aluminium of the box. The material properties and parameters used are shown in Table 1.

Material	$\rho(\text{kg/m}^3)$	E (GPa)	ν	A (GPa)	B (GPa)	n	C	M	D ₁
6063-T5	2700	71	0.33	0.2	0.144	0.62	0	1	0.2

Table 1: The material properties and parameters used in *MAT_015

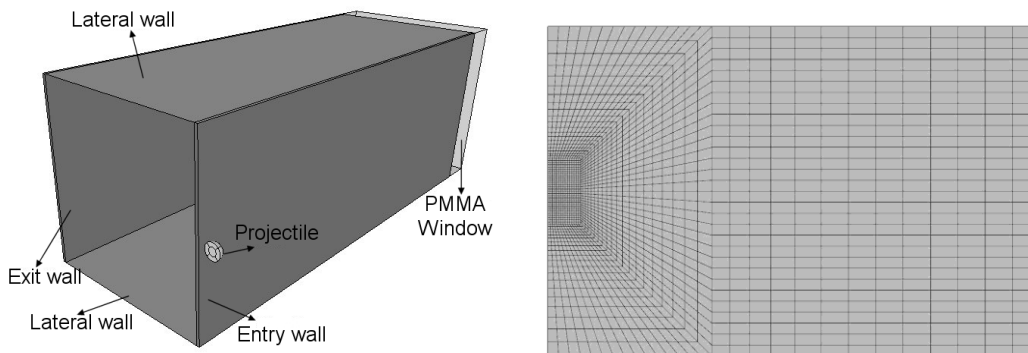


Fig.3: Tube model. Left: Components of the model (Half tub). Right: Mesh detail of the impacted walls.

3.1.2 CFRP tube

The woven CFRP tube is discretised by means of eight node linear solid elements with reduced integration and hourglass control. The mesh is more refined in the impacted zone ($1 \times 1 \text{ mm}^2$) than far from the impact point, obtaining a mesh that accurately reproduces the damage induced according to previous works [8]. The CFRP tube walls present 10 elements through thickness, so each element corresponds to one ply.

The behavior of the carbon/epoxy woven laminate takes into account intra-laminar and inter-laminar damage. The former has been modelled as an orthotropic elastic material until failure, implemented through a user subroutine; whilst for the later, a cohesive interaction is used. These kind of approaches have been widely used in impact problems on composite materials [9-12]. In the CFRP model, two failure mechanisms are considered: fiber failure and matrix failure. Different failure variables d_i (based on stresses) are defined for each failure mechanism. When the value of any of these variables reaches the value of 1, failure initiates and all the components of the stress tensor σ_{ij} involved in the failure definition, are set to zero. In addition, an element removal criteria is used, based on total strain. The mechanisms are:

1. Fibre failure. Due to woven configuration, fiber failure can appear in the two in-plane axes. The fiber failure criteria are described by means of d_{f1} and d_{f2} , one for each direction:

$$d_{f1} = \begin{cases} \frac{\sigma_{11}}{X_t} & \text{if } \sigma_{11} > 0 \\ \frac{|\sigma_{11}|}{X_c} & \text{if } \sigma_{11} < 0 \end{cases} \quad (1)$$

$$d_{f2} = \begin{cases} \frac{\sigma_{22}}{Y_t} & \text{if } \sigma_{22} > 0 \\ \frac{|\sigma_{22}|}{Y_c} & \text{if } \sigma_{22} < 0 \end{cases} \quad (2)$$

Where X_t and X_c are the strengths of the composite laminate in tension and compression for the warp direction, and finally Y_t and Y_c are the strengths in tension and compression for the fill direction.

2. Matrix failure. The matrix failure distinguished two mechanisms: in-plane shear (d_{m12}) and out-plane crushing (d_{m3}).

$$d_{m12} = \frac{\sigma_{12}}{S_{12}} \quad (3) \quad d_{m3} = \frac{1}{4} \left(\frac{\sigma_{33}}{S_{13}} \right)^2 + \frac{Z_c \cdot \sigma_{33}}{4S_{13}S_{23}} + \left| \frac{\sigma_{33}}{Z_c} \right| + \max \left[\left(\frac{\sigma_{13}}{S_{13}} \right)^2, \left(\frac{\sigma_{23}}{S_{23}} \right)^2 \right] \quad (4)$$

where S_{12} , S_{13} and S_{23} are the shear strengths in the three different planes and Z_c is the strength in the through-thickness direction under compression. Eq. (4) applies only when $\sigma_{33} < 0$.

The properties of the carbon fibre woven laminates are presented in Table 2.

Elastic properties					
$E_1=E_2$ 68 GPa	E_3 10 GPa	ν_{12} 0.22	$\nu_{13}=\nu_{23}$ 0.49	G_{12} 5 GPa	$G_{23}=G_{13}$ 4.5 GPa
Strength Properties					
$X_t=Y_t=X_c=Y_c$ 880 MPa	Z_c 340 MPa	Z_r 96 MPa	S_{12} 84 MPa	S_{13} 120 MPa	S_{23} 120 MPa
Maximum strain					
ϵ_{12} 0.025	ϵ_3 0.05	$\epsilon_{12}=\epsilon_{23}=\epsilon_{13}$ 0.1			

Table 2: Properties of woven carbon/epoxy laminate.

Inter-laminar damage is modelled through a cohesive surface interaction. The cohesive behaviour is based on a traction-separation law, in which is necessary to define a damage initiation criteria and a damage evolution law. This is achieved choosing the option 9 of the LS-DYNA contact card: ***CONTACT_AUTOMATIC_SURFACE_TO_SURFACE_TIEBREAK**. The parameters for the cohesive interface are shown in Table 3.

E_N	E_T	T	S	G_{IC}	G_{IIC}	M
40 GPa	30 GPa	11 MPa	45 MPa	287 J/m ²	1830 J/m ²	1.42

Table 3: Parameters of the cohesive interface.

Finally, in both cases, the projectile that impacts on the corresponding tube and the PMMA window were discretised by means of eight node conventional solid elements with reduced integration. The steel projectile ($\rho = 7850 \text{ kg/m}^3$; $E = 210 \text{ GPa}$; $\nu = 0.3$) and the PMMA window ($\rho = 1180 \text{ kg/m}^3$; $E = 3 \text{ GPa}$; $\nu = 0.35$) were modelled as elastic materials since no plastic deformation nor damage were observed in none of them in the experimental tests.

3.2 Fluid Models

The same numerical modelling, regarding the fluids, was implemented for the impacts on Aluminium and CFRP tubes.

3.2.1 MM-ALE approach

The fluid inside the box is discretised by means of eight-node solid hexahedron elements with an ALE formulation (***SECTION_SOLID**, $\text{elform} = 11$). In this case, the air surrounding the box was also considered, being modeled using the same elements as in the water. Modelling this air region is essential to allow the water to flow into it, deforming the walls of the structure. This is only possible if the water and air meshes share the same nodes at their interface. Four discretization densities were analysed in order to achieve an optimal mesh density. The results in terms of projectile deceleration were compared with the classical solution of the movement of a sphere inside a liquid. Finally, the mesh size was selected in order to match with the Lagrangian one at the interfaces. This helped to control the leakage problems.

The water and the air were both modelled using the `*MAT_NULL` (MAT_009) and a `*EOS_MIE_GRUNEISEN` for the water and a `*EOS_LINEAR_POLYNOMIAL` for the air. Table 4 shows the parameters used in the mentioned cards.

	$\rho_0(\text{kg/m}^3)$	$\nu_d(\text{Pa s})$	$C(\text{m/s})$	S_1	S_2	S_3	γ_0	a	C_4	C_5	$E_0(\text{J/m}^3)$
Water	1000	0.89e-03	1448	1.979	0	0	0.11	3.0	-	-	-
Air	1.22	1.77e-05	-	-	-	-	-	-	0.4	0.4	2.53e5

Table 4: Water and Air parameters used in the simulations for MM-ALE and SPH approaches.

The fluid–structure interaction, for both projectile/fluid and walls/fluid, is achieved by means of a penalty-based ALE–Lagrangian coupling algorithm implemented within LS-DYNA (`*CONSTRAINED_LAGRANGE_IN_SOLID`).

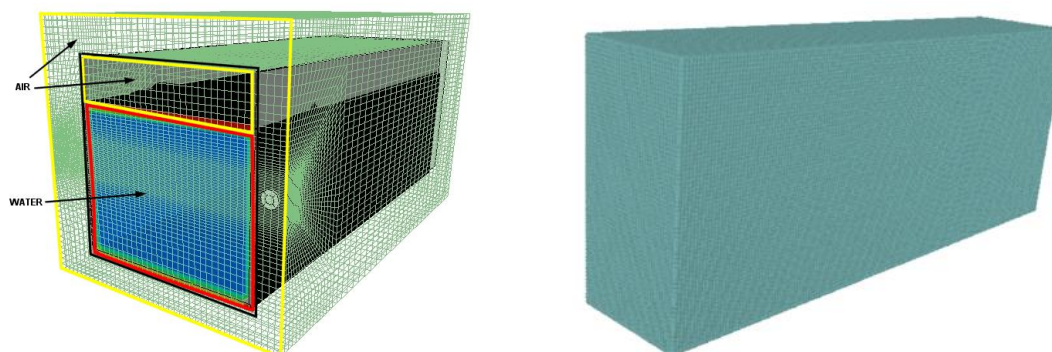


Fig.4: Left: MM-ALE model for a partially fluid filled tube. Right: SPH fluid model

3.2.2 SPH approach

In this case, the fluid inside the box is discretised by means of a set of particles assigned with a mass interacting among themselves without a direct connectivity (`*SECTION_SPH`). The SPH method requires a large number of particles uniformly distributed to provide reasonably accurate results. In the SPH method, it is not necessary to model the surrounding air since the particles can freely flow in any direction deforming the walls of the structure. The material model and the equation of state used for the water were the same as in the ALE approach (Table 4).

This time, the fluid–structure coupling algorithm is different from the one applied with the ALE approach. For the interaction with the projectile, a penalty-based `*NODE_TO_SURFACE` contact interface has been used. The contact interface was chosen with special care in order to achieve the interaction of several SPH particles with each face of the elements of the Lagrange contacting body. This fact, linked to the necessity of a homogenous mesh to obtain accurate results, leads to a higher number of particles to discretise the water domain than in the ALE approach. The interaction of the SPH particles and the walls of the structure was made by means of a constraint interface that ties the SPH particles to the solid elements of the surrounding structure (`*CONTACT_TIED_NODES_TO_SURFACE`). This has been proven as the best way to transmit the fluid movement to the structure and avoid contact instabilities.

4 Validation

The numerical results are compared qualitative and quantitatively to the experimental data.

1. Projectile position. The experimental projectile position, obtained by means of a high-speed camera, can be compared with the numerical data. The experimental and numerical time history of the projectile show a good correlation, for both MM-ALE and SPH approaches. The trend of the projectile velocity can be observed by means of the projectile position slope. The velocity decreases inside the fluid, transforming part of its kinetic energy into pressure and kinetic energy in

the fluid. It was observed that the projectile position inside the fluid was not affected for the fluid filled volume, so neither the energy transfer between fluid and projectile.

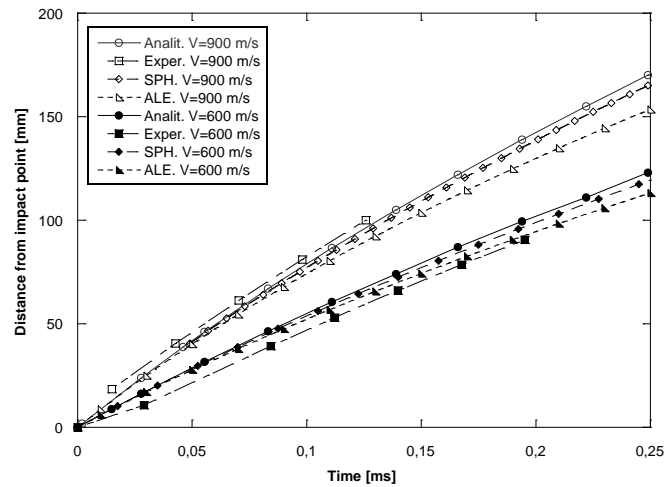


Fig.5: Projectile position time history in a 100% filled tube impacted at different velocities.

2. HRAM phenomenon. As an example of the qualitative comparisons carried out, Fig. 6 shows images of the penetration process when a projectile impacts at 600 m/s into a tank filled at 60%, both experimental and numerical. For a better representation of the phenomenon in the numerical simulations, the pressure contours are depicted. It can be seen how the numerical approaches, MM-ALE and SPH, qualitatively reproduce the main characteristics of an HRAM event. Firstly, a hemispherical pressure wave is generated by the impact. Then, this pressure wave travels at the sound velocity through the fluid, while the drag force decelerates the projectile creating a cavity in the wake and an overpressure just ahead the projectile. The cavity grows and pushes the layer of fluid that initially is above the projectile trajectory. The overpressure of the fluid ahead the projectile will cause a pre-stress situation in the exit wall that will generate a higher damage than in the entry wall. Finally, the cavity continues growing and the layer of fluid approaches the upper wall. The same comparison can be done in all the considered cases.

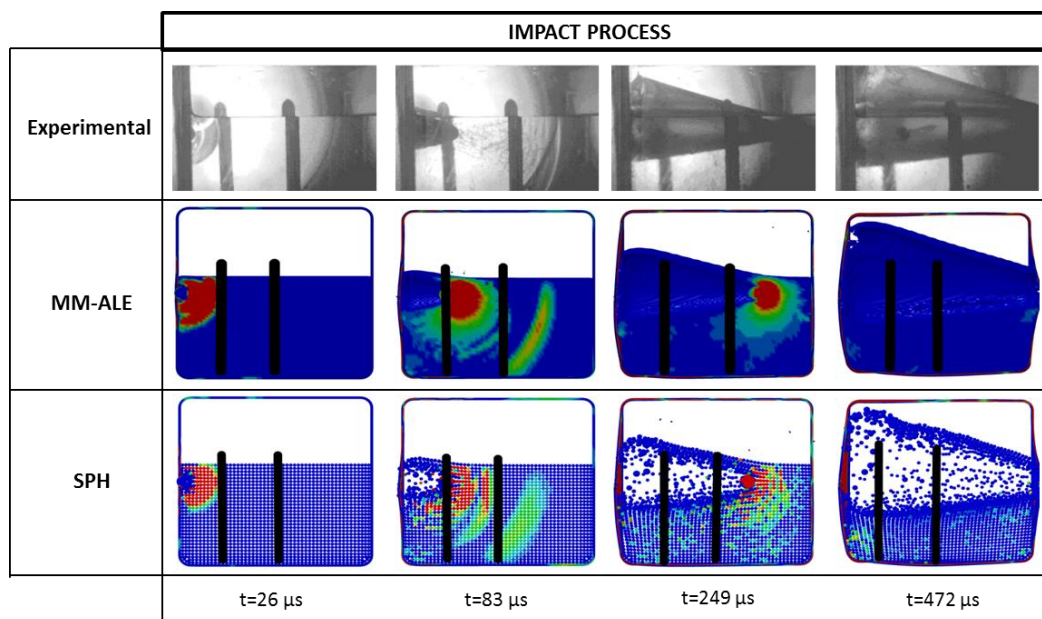


Fig.6: Penetration process in a partially filled tube.

3. Pressure field. The experimental pressure data in two different points of the fluid (PTn, near the impact point and PTf, far from impact point) were compared with the numerical results. The pressure curves, both experimental and numerically (MM-ALE and SPH), shows a good correlation in all the cases, not only in peak values but in the trends regarding pressure transducer location influence.

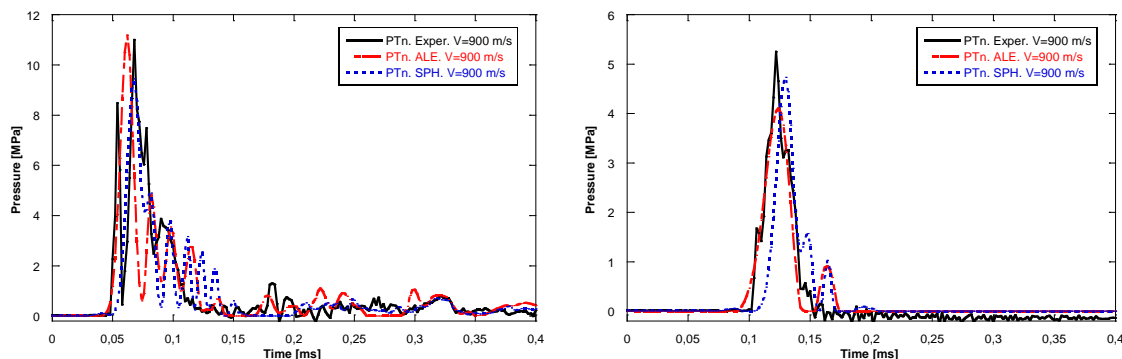


Fig.7: Pressure time history in a 100% filled tube impacted at 900 m/s. Left: PTn. Right: Ptf

4. Deformations in aluminium tube walls. Experimental deformation data in the entry and exit walls of the tubes were compared with the simulation results. In all the cases, it is observed that the maximum deformation is quite well predicted in the simulations. In addition, it was seen that the shape in the nearest area to impact (about 15 cm at both sides of the impact point) is well represented in the simulations, whereas the deformation at points far from the impact point is overestimated in the simulations. As an example, Fig.8 depicts the deformation of the entry and exit walls, all along the tube impacted at 600 m/s.

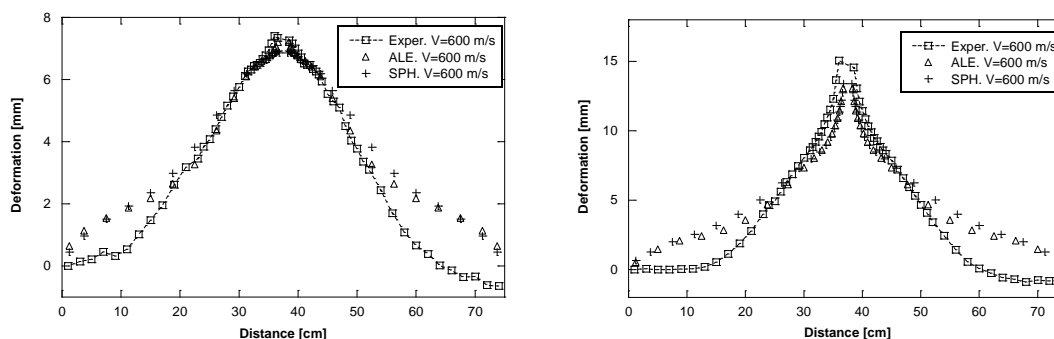


Fig.8: Displacement of the walls in a 100% filled tube. Left: Entry wall. Right: Exit wall

5. Failure in CFRP tubes. The failures that appear numerically in the CFRP tubes were compared qualitatively with the experimental results. Fig. 9 shows the main failures, which appear on the upper and exit walls, of a partially filled CFRP tank impacted at 900 m/s. It can be seen that the exit wall presents a cross-type failure that is well predicted by the numerical approaches for both fluid filled levels. The failure on the upper wall is due to the impact of the layer of fluid that is raised by the projectile; it begins in the border of the exit wall and then advances through the upper wall. This kind of failure only appears in partially filled cases and is higher for the case of 75% than in 60%. Both numerical methods reproduce the failure on the border and its length but not the propagation through the wall. However, despite the complexity of this process and that the influence of CFRP manufacturing in the tube behaviour makes difficult to reproduce same experimental failures in numerical simulation, similar trends can be seen in both experimental and numerical final failures.

More details about the experiments, numerical models and validation performed as well as the analysis of the HRAM phenomenon can be found in the works of Varas et. al. [5,6,13,14,15] and Artero-Guerrero et al. [16]

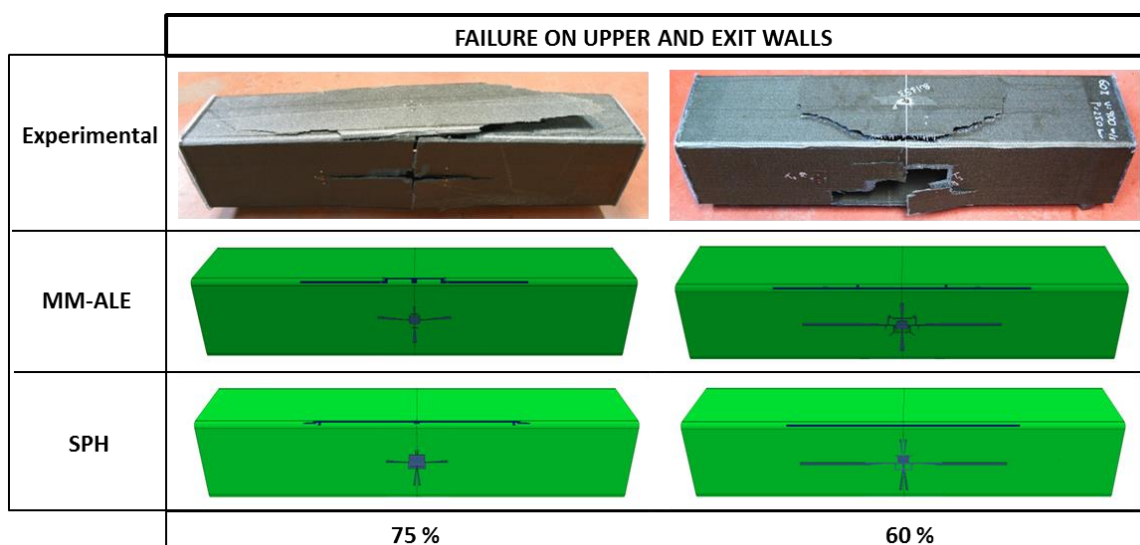


Fig.9: Failure of upper and exit walls of a CFRP tube impacted at 900 m/s.

5 HRAM attenuation simulations.

Once the numerical model is validated, it can be used to perform simulations in order to study different possibilities to attenuate the HRAM effects on the structures. The effects of the HRAM phenomenon on the structures are basically due to two mechanisms: the pressure wave generated by the impact and the cavity evolution. Therefore, if one or both mechanisms can be controlled or reduced, it is reasonable to think that the HRAM effect would be mitigated. To study how this two mechanisms influence the structural response of this kind of tubes, different simulations adding inside an aluminium tube, both metallic plates and thin sandwich structures (with two metallic skins and an air core or buffer) have been performed, Table 5. The results obtained have been compared with the results of the case in which no plate is inside the fluid (reference model), previously detailed.

Plates parallel to impacted walls				
Case	Number of plates	Plate thickness	Air buffer	Distance from impact point
1	0	-	No	-
2	1	1 mm		45 mm
3				100 mm
4	2			45 and 100 mm
5	2		Yes	45 mm
6		100 mm		
7	4	45 and 100 mm		
8		35 and 110 mm		

Table 5: Cases studied for the attenuation of HRAM

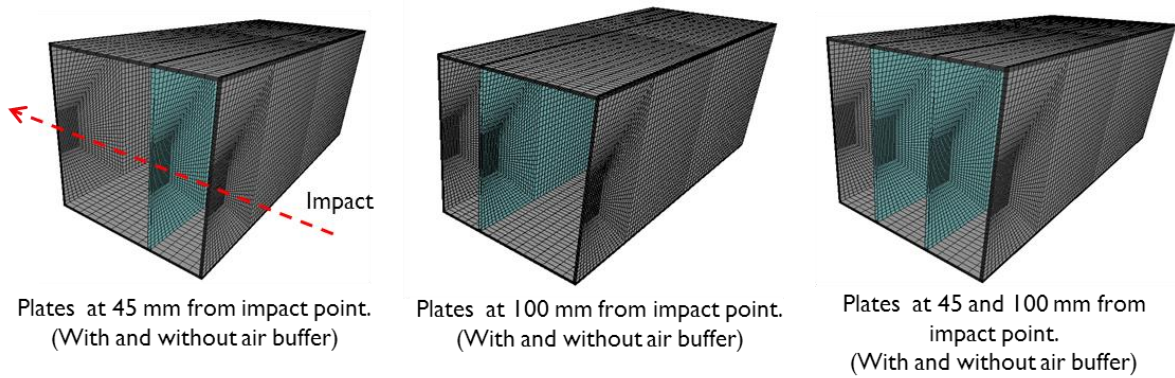


Fig.10: Different tube models with metallic plates inside the tube (with and without air buffer)

5.1 Results and conclusions

Some of the main results obtained in the simulations are showed below.

5.1.1 Cavity evolution

Differences in the cavity evolution between the reference model and the cases with and without air buffer can be observed in Fig. 11, where the volume fraction is depicted. It can be seen that the case in which the air buffers are included, the cavity presents a smaller growing and hence, its reduction occurs before than in the other cases. Therefore it is reasonable to think that the effects on the walls will less serious than in the other cases.

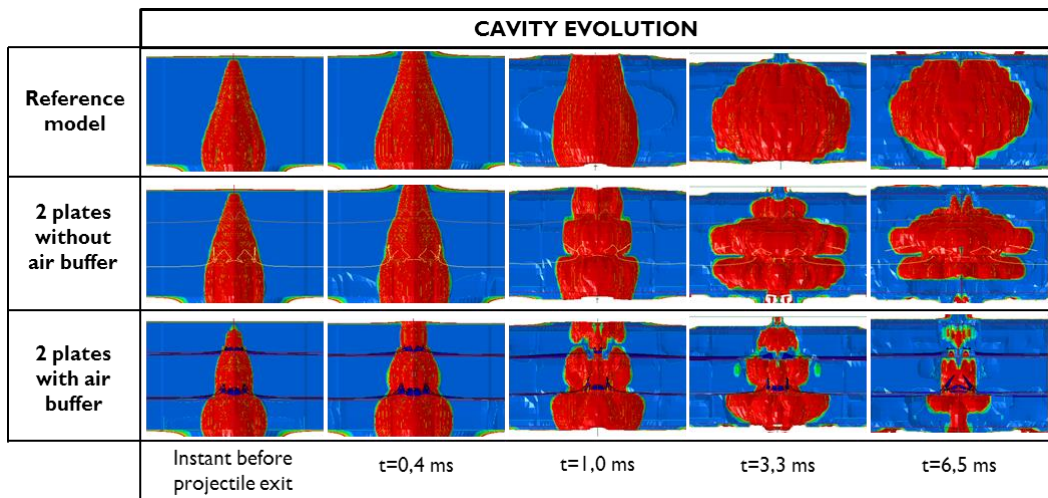


Fig.11: Cavity evolution on a 100% filled tube impacted at 900 m/s.

5.1.2 Pressure wave

The propagation of the pressure wave is shown in Fig. 12. It is clearly observed how in the case with the air buffers the pressure wave is stopped when reaches the air interfaces, helping to reduce the pressure inside the tube.

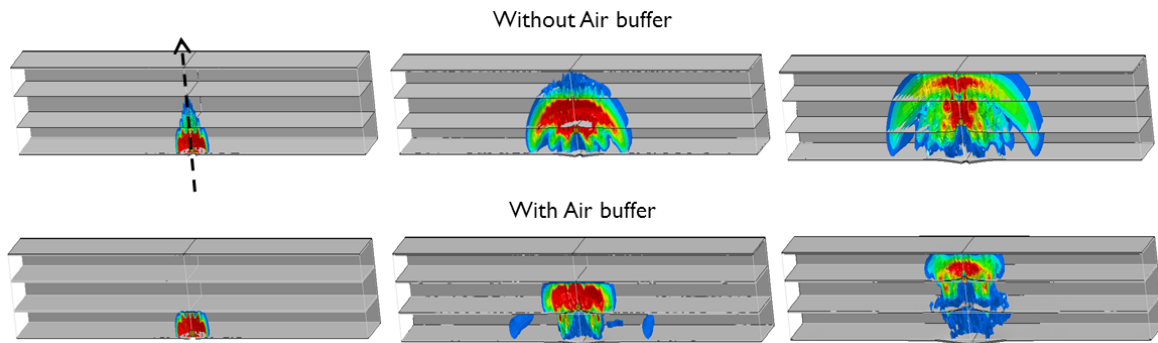


Fig.12: Pressure wave evolution in a completely filled tube impacted at 900 m/s

5.1.3 Pressure time history

The pressure time history in two points inside the fluid, one point near the impact wall (PTn) and other far from the impact wall (PTf), is shown in Fig.13. It can be seen how the air buffer models help to diminish the peak pressure values on those points.

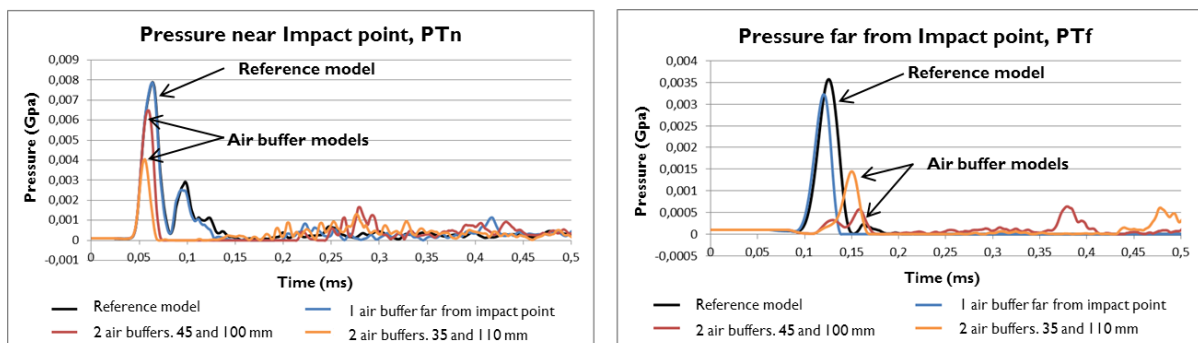


Fig.13: Pressure time history in a completely filled tube impacted at 900 m/s

5.1.4 Displacement of the walls

Finally, the effects of the HRAM on the impacted walls is shown in Fig. 14. It can be clearly observed that previous results, regarding the smaller cavity evolution and the reduction in the pressure values, obtained in the air buffer cases lead to a smaller displacement of the tube walls.

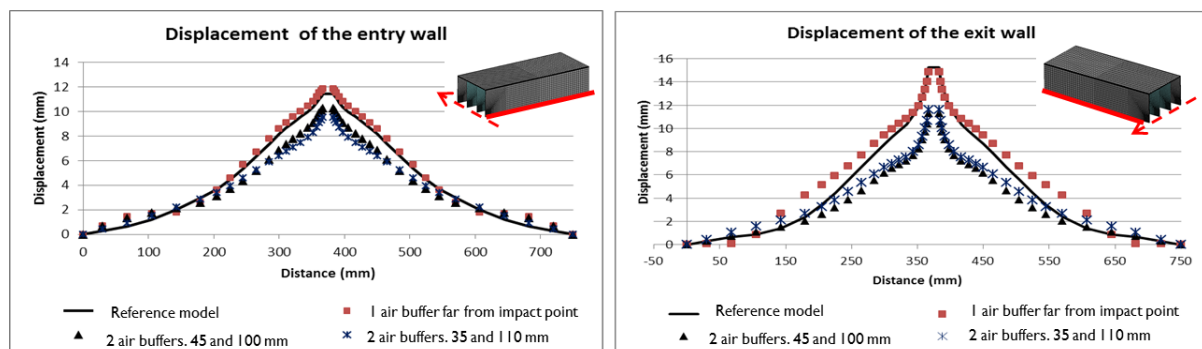


Fig.14: Displacement of the impacted walls of a completely filled tube impacted at 900 m/s

Attending to the results obtained, it can be said that the air buffering option could be a possibility to attenuate the HRAM phenomenon effects on this kind of structures. Nevertheless a deeper study is needed to analyze more cases and to completely understand the physics of the problem.

6 Summary

Both approaches ALE and SPH are capable of faithfully reproducing the four well known stages of the hydrodynamic ram: shock, drag, cavitation and exit phases from a qualitative and quantitative perspective. The cavity evolution, main cause of the tank final deformation, is accurately reproduced as compared with the images taken from the experimental tests. Hence, the effects of the HRAM in a metallic and a composite laminate structure are well predicted by both numerical approaches.

The SPH mesh requires a much higher computation effort. This fact, added to the need of a constant size of the particles along the fluid, results in better ratio accuracy by computation time with the ALE mesh. In the case of problems in which the analysed domain is relatively small, the use of SPH meshes could be an appropriate choice; differences in computation efforts between ALE and SPH diminish with the number of elements (or particles).

The addition of metallic plates, forming a sandwich with an air core as a buffer, inside the tubes could be a possible solution to attenuate the HRAM effects. Nevertheless, more simulations and a deeper study need to be done for a better understanding of the phenomena.

7 References

- [1] Airoldi A. and Cacchione B., Modelling of impact forces and pressures in Lagrangian bird strike analysis, *Int. J. Impact Engineering*, Vol.32 (2006), p.1651
- [2] Anghileri M., Castelletti LML, Invernizzi F. and Mascheroni M, A survey of numerical models for hail impact analysis, *Int. J. Impact Engineering*, Vol.31 (2005), p.929
- [3] Mines RAE, McKown S and Birch RS, Impact of aircraft rubber tyre fragments on aluminium alloy plates: I-experimental, *Int. J. Impact Engineering*, Vol.34 (2007), p.626
- [4] Pernas-Sánchez J, Pedroche D.A., Varas D, López-Puente J and Zaera R., Numerical modeling of ice behavior under high velocity impacts. *Int. J. of solids and structures*, Vol. 49 (2012), p.1919
- [5] Varas D., López-Puente J. and Zaera R., Experimental analysis of fluid-filled aluminium tubes subjected to high-velocity impact. *Int. J. Impact Engineering*, Vol.36 (2009), p.81
- [6] Varas D, Zaera R. and López-Puente J, Experimental study of CFRP fluid-filled tubes subjected to high-velocity impact. *Composite Structures*, Vol.93 (2011), p.2598
- [7] LS-DYNA Users Manual, Version 971, Livermore Software Technology Corporation, May 2007
- [8] López-Puente J, Zaera R, Navarro C., High energy impact on woven laminate. *J.Phys IV* 2003;110:639–44.
- [9] Hou JP, Petrinic N, Ruiz C, Hallett SR., Prediction of impact damage in composite plates., *Compos Sci Technol* 2000;60(2):273–81.
- [10] López-Puente J, Zaera R, Navarro C., Experimental and numerical analysis of normal and oblique ballistic impacts on thin carbon/epoxy woven laminates., *Compos Part A – Appl S* 2008;39:374–87.
- [11] Camanho PP, Davila CG. Mixed-Mode decohesion finite elements for the simulation of delamination in composite materials. Tech Report NASA/TM-2002-211737 2002:1-37.
- [12] Turon A, Camanho PP, Costa J, Renart J. Accurate simulation of delamination growth under mixed-mode loading using cohesive elements: definition of interlaminar strengths and elastic stiffness. *Compos. Struct.* 2010;92(8):1857–64.
- [13] Varas D, Zaera R. and López-Puente J, Numerical modeling of the hydrodynamic ram phenomenon. *Int. J. Impact Engineering*, Vol.36 (2009), p.363
- [14] Varas D., López-Puente J. and Zaera R. Numerical analysis of the hydrodynamic ram phenomenon in aircraft fuel tanks. *AIAA Journal*, Vol.50 (2012), p.1621
- [15] Varas D, Zaera R. and López-Puente J, Numerical modelling of partially filled aircraft fuel tanks submitted to Hydrodynamic Ram, *Aerospace Science and Technology*, vol. 16, (1), 2012. P. 19-28
- [16] Artero-Guerrero, J. A., Pernas-Sánchez, J., López-Puente, J., Varas, D., On the influence of filling level in CFRP aircraft fuel tank subjected to high velocity impacts, *Composite Structures*, vol. 107, January, pp. 570-577.